

VARIATIONAL MESH ADAPTATION METHODS FOR AXISYMMETRICAL PROBLEMS*

WEIMING CAO[†], RICARDO CARRETERO-GONZÁLEZ[‡], WEIZHANG HUANG[§], AND
ROBERT D. RUSSELL[¶]

Abstract. We study variational mesh adaptation for axially symmetric solutions to two-dimensional problems. The study is focused on the relationship between the mesh density distribution and the monitor function and is carried out for a traditional functional that includes several widely used variational methods as special cases and a recently proposed functional that allows for a weighting between mesh isotropy (or regularity) and global equidistribution of the monitor function. The main results are stated in Theorems 4.1 and 4.2. For axially symmetric problems, it is natural to choose axially symmetric mesh adaptation. To this end, it is reasonable to use the monitor function in the form $G = \lambda_1(r)e_r e_r^T + \lambda_2(r)e_\theta e_\theta^T$, where e_r and e_θ are the radial and angular unit vectors.

It is shown that when higher mesh concentration at the origin is desired, a choice of λ_1 and λ_2 satisfying $\lambda_1(0) < \lambda_2(0)$ will make the mesh denser at $r = 0$ than in the surrounding area whether or not λ_1 has a maximum value at $r = 0$. The purpose can also be served by choosing λ_1 to have a local maximum at $r = 0$ when a Winslow-type monitor function with $\lambda_1(r) = \lambda_2(r)$ is employed. On the other hand, it is shown that the traditional functional provides little control over mesh concentration around a ring $r = r_\lambda > 0$ by choosing λ_1 and λ_2 .

In contrast, numerical results show that the new functional provides better control of the mesh concentration through the monitor function. Two-dimensional numerical results are presented to support the analysis.

Key words. mesh adaptation, variational method, mesh regularity, equidistribution

AMS subject classifications. 65M50, 65M60

PII. S0036142902401591

1. Introduction. Mesh adaptation has become an indispensable tool for use in the numerical solution of PDEs. One of the most widely used approaches for generating adaptive meshes is a variational method. With such a method, meshes are generated as images of a reference mesh through a coordinate transformation between the physical and computational (or logical) domains. The transformation is determined as the minimizer of a functional formulated to measure difficulties in the numerical approximation of the physical solution, typically through a so-called monitor function prescribed by the user to control the mesh adaptation. A variational method often results in an elliptic (PDE) mesh generation system. Such a system generates smooth meshes, allows for full specification of mesh behavior at the boundary, does not propagate boundary singularities into the domain, has less danger of producing mesh overlappings, and can be solved efficiently using many well-developed

*Received by the editors January 28, 2002; accepted for publication (in revised form) September 23, 2002; published electronically March 19, 2003. This work was supported in part by NSF (USA) grant DMS-0074240, and NSERC (Canada) grant OGP-0008781.

<http://www.siam.org/journals/sinum/41-1/40159.html>

[†]Department of Mathematics, The University of Texas at San Antonio, San Antonio, TX 78249 (wcao@math.utsa.edu).

[‡]Department of Mathematics, Simon Fraser University, Burnaby, BC V5A 1S6, Canada. Current address: Nonlinear Dynamical Systems Group, Department of Mathematics and Statistics, San Diego State University, San Diego, CA 92182 (carreter@math.sdsu.edu).

[§]Department of Mathematics, the University of Kansas, Lawrence, KS 66045 (huang@math.ukans.edu).

[¶]Department of Mathematics, Simon Fraser University, Burnaby, BC V5A 1S6, Canada (rdr@cs.sfu.ca).

algorithms. Moreover, the equidistribution principle, a concept which has been used successfully in one-dimensional mesh adaptation [3], can be naturally extended to multidimensions in the variational framework. Finally, many mesh features, such as orthogonality, smoothness, and concentration, can be incorporated explicitly into the mesh adaptation functional.

A number of variational methods have been developed in the past. For example, Winslow [15] proposes the variable diffusion method for which the mesh lines play the role of equipotentials of a potential problem [14]. Brackbill and Saltzman [1] develop a popular method combining mesh concentration, smoothness, and orthogonality. Several functionals are formulated by Steinberg and Roache [13] to control mesh properties such as the spacing of the points, areas or volumes of the cells, and the angles between mesh lines. Dvinsky [4] uses the energy of harmonic mappings as his mesh adaptation functional. Knupp [9, 10] and Knupp and Robidoux [11] develop functionals based on the idea of conditioning the Jacobian matrix of the coordinate transformation. A functional balancing mesh regularity and adaptivity is proposed by Huang [6].

Some theoretical work has been devoted to better understanding the existing methods. Cao, Huang, and Russell [2] study the qualitative effect of monitor functions on the resulting mesh for a general class of variational methods that includes Winslow's method [15] and the method using harmonic mappings [4] as special cases. In the recent work of Huang and Sun [8], the monitor function for the functional of [6] is defined based on interpolation error estimates, and asymptotic error bounds are obtained for interpolation on the resulting adaptive meshes satisfying the so-called isotropy and equidistribution conditions. The ability of the resulting method to generate adaptive meshes satisfying these conditions is also demonstrated numerically. Nevertheless, more work remains to be done on better understanding the existing variational methods, especially on precisely how the monitor function controls the concentration of the generated mesh.

In this paper we present such a study for two functionals, the traditional one studied in [2] and the new one proposed in [6], for the simple but important case of two-dimensional problems with axisymmetrical solutions. These types of problems arise in many practical situations, particularly for problems with blowup or quenching solutions. There has been considerable recent interest in solving higher-dimensional blowup problems such as the Schrödinger equation, and this work was motivated by the observation that the standard moving mesh procedures generally perform inadequately on such problems (e.g., see [2, 12]).

Let (x, y) be the coordinates in the physical domain Ω , and let (ξ, η) be the coordinates in the computational domain Ω_c . The traditional functional is

$$(1.1) \quad I_{trad}[\xi, \eta] = \int_{\Omega} (\nabla \xi^T G^{-1} \nabla \xi + \nabla \eta^T G^{-1} \nabla \eta) \, dx dy$$

and the new functional in [6] has the form

$$(1.2) \quad \begin{aligned} I_{new}[\xi, \eta] &= \gamma \int_{\Omega} \sqrt{g} (\nabla \xi^T G^{-1} \nabla \xi + \nabla \eta^T G^{-1} \nabla \eta)^q \, dx dy \\ &+ (1 - 2\gamma) 2^q \int_{\Omega} \frac{\sqrt{g}}{(J\sqrt{g})^q} \, dx dy, \end{aligned}$$

where $J = x_{\xi}y_{\eta} - x_{\eta}y_{\xi}$ is the Jacobian of the coordinate transformation, G is the (matrix) monitor function with determinant g , and $q \geq 1$ and $\gamma \in (0, 1/2]$ are pa-

rameters. Here, $q \geq 1$ is required in order for the first integral of (1.2) to be convex. The features of these functionals and the roles of the parameters will be discussed in sections 2 and 3.

Axisymmetrical problems. For simplicity, we assume that the physical domain is $\Omega = \{(x, y) \mid x^2 + y^2 < 1\}$ and the computational domain is $\Omega_c = \{(\xi, \eta) \mid \xi^2 + \eta^2 < 1\}$. Let the polar coordinate systems for the physical and computational domains be

$$\begin{cases} x = r \cos \theta, \\ y = r \sin \theta, \end{cases} \quad \begin{cases} \xi = R \cos \Theta, \\ \eta = R \sin \Theta. \end{cases}$$

Consider the case where the solution $u(x, y)$ is axially symmetric; i.e., u is invariant under rotation about the center $(0, 0)$. It is natural to choose an axially symmetric coordinate transformation

$$(1.3) \quad R = R(r), \quad \Theta = \theta$$

for mesh adaptation. To this end, it is reasonable to use the monitor function in the form

$$(1.4) \quad G = \lambda_1(r) \mathbf{e}_r \mathbf{e}_r^T + \lambda_2(r) \mathbf{e}_\theta \mathbf{e}_\theta^T,$$

where \mathbf{e}_r and \mathbf{e}_θ are unit vectors in the radial and angular directions, respectively. Thus, G is determined by its radial and angular components $\lambda_1 > 0$ and $\lambda_2 > 0$.

We are interested in the relationship between the monitor function and the mesh distribution. In particular, we focus on the mesh density $D(r)$. The Jacobian of the coordinate transformation J is easily seen to satisfy

$$(1.5) \quad \frac{1}{J} \equiv \det \begin{pmatrix} \partial(\xi, \eta) \\ \partial(x, y) \end{pmatrix} = \frac{R}{r} \frac{dR}{dr},$$

and thus the mesh density is given by

$$(1.6) \quad D(r) = \frac{R}{r} \frac{dR}{dr}.$$

The central aim of this paper is to gain insight into how much control one has on the mesh density $D(r)$ by appropriately choosing λ_1 and λ_2 . In order for the variational method to be successful one needs that the solution to the variational problem gives a mesh distribution compatible with the chosen monitor function. For example, it is natural to choose one or more of the eigenvalues of the monitor function to have a higher value (a maximum) in the region where a physical solution needs a high concentration of mesh points; e.g., see [2]. It will become clear below that this is not always achievable and that if one is not careful in choosing the appropriate relation between λ_1 and λ_2 it is possible for the mesh density maximum to occur at a different location than that of the maximum of the eigenvalue. This can in turn lead to a large error in the numerical approximation of the physical solution.

An outline of the paper is as follows. In sections 2 and 3 basic properties of the traditional and new functionals for radially symmetric problems are presented. In section 4 we carry out an in-depth analysis on the control of the mesh density via the monitor function. In particular, we find that the relationship between the radial (λ_1) and the angular (λ_2) components of the monitor function is crucial for a good control of the mesh density. Section 5 presents some two-dimensional numerical results highlighting in part the lack of control of the mesh concentration for a wide choice of monitor functions. A brief analysis is given in section 6 for the traditional functional applied to spherically symmetric problems in three dimensions. Finally, section 7 contains conclusions and comments.

2. The traditional functional. In this section we consider the traditional functional (1.1) for axisymmetrical problems and give some of its basic properties. It is a generalization of the functionals for Winslow's method and Dvinsky's method of harmonic mappings. The monitor function G can be defined by arbitrarily choosing λ_1 and λ_2 . However, it is worth pointing out that a number of commonly used monitor functions can be obtained through the interdependent relationship

$$(2.1) \quad \lambda_2 = \lambda_1^p$$

for some power p . For example, we have

$$(2.2) \quad \begin{array}{ll} \text{(HM)} & p = -1 : \quad \text{harmonic mapping monitor function;} \\ \text{(Al)} & p = 0 : \quad \text{arclength monitor function;} \\ \text{(Ws)} & p = 1 : \quad \text{Winslow's monitor function;} \\ \text{(St)} & p = 2 : \quad \text{strong concentration monitor function.} \end{array}$$

In polar coordinates the gradient operator reads as

$$\nabla = \mathbf{e}_r \frac{\partial}{\partial r} + \frac{\mathbf{e}_\theta}{r} \frac{\partial}{\partial \theta},$$

and it follows from (1.3) and (1.4) that

$$(2.3) \quad \nabla \xi^T G^{-1} \nabla \xi + \nabla \eta^T G^{-1} \nabla \eta = \frac{1}{\lambda_1} \left(\frac{dR}{dr} \right)^2 + \frac{1}{\lambda_2} \left(\frac{R}{r} \right)^2.$$

Substituting (2.3) into (1.1) gives

$$I_{\text{trad}}[R] = 2\pi \int_0^1 \left[\frac{1}{\lambda_1} \left(\frac{dR}{dr} \right)^2 + \frac{1}{\lambda_2} \left(\frac{R}{r} \right)^2 \right] r dr,$$

and its Euler-Lagrange equation is

$$(2.4) \quad -\frac{d}{dr} \left(\frac{r}{\lambda_1} \frac{dR}{dr} \right) + \frac{R}{r\lambda_2} = 0.$$

This equation is supplemented with the boundary conditions

$$(2.5) \quad R(0) = 0, \quad R(1) = 1.$$

For a given monitor function (i.e., for given λ_1 and λ_2), solving (2.4) determines the resulting mesh transformation $R(r)$.

2.1. Nonnegativeness and mesh crossing. We have $R(r) \geq 0$ for $r \in (0, 1)$. To see this, we note that the minimum of $R(r)$ occurs at the left end and/or an interior point due to the boundary conditions (2.5). If $R(0) = \min R(r)$, then we have $R(r) \geq 0$ from (2.5). If instead the minimum point is $r_0 \in (0, 1)$, then $R'(r_0) = 0$ and $R''(r_0) \geq 0$. From (2.4)

$$\frac{1}{r_0 \lambda_2} R(r_0) = \frac{d}{dr} \left(\frac{r}{\lambda_1} \right) \left(\frac{dR}{dr} \right) \Big|_{r_0} + \frac{r}{\lambda_1} \frac{d^2 R}{dr^2} \Big|_{r_0} \geq 0.$$

Hence, in either case $R(r) \geq R(r_0) \geq 0$. Furthermore, (2.4) gives

$$\frac{dR}{dr} = \frac{\lambda_1}{r} \int_0^r \frac{R(x)}{x \lambda_2(x)} dx,$$

so it follows that $\frac{dR}{dr} > 0$ for $r \in (0, 1)$; i.e., the mesh transformation is guaranteed to be nonsingular and produce no mesh crossing.

2.2. Mesh transformation for harmonic mappings. For the case of harmonic mappings ($p = -1$ or $\lambda_2 = 1/\lambda_1$) it is possible to find an analytical form for the mesh transformation $R(r)$. We explicitly construct $R(r)$ here since it then serves as the basis of study for other cases. Using the change of coordinates

$$(2.6) \quad s(r) = \int_1^r \frac{\lambda_1(x)}{x} dx,$$

(2.4) reads

$$-\frac{d^2 R}{ds^2} + R = 0.$$

Its solution satisfying the boundary conditions (2.5) is $R(r) = e^s$. In section 4.1, using a transformation based on (2.6), we study more general monitor functions (including arclength and Winslow) in detail.

3. The new functional. The formulation of the new functional (1.2) is based on the so-called isotropy (or regularity) and equidistribution (or adaptation) requirements for an error distribution [6]. Specifically, the first integral term corresponds to the regularity requirement, while the second is associated with equidistribution. These two requirements are balanced by adjusting the value of the parameter γ . When $q = 1$ or $\gamma = 1/2$, the second integral becomes constant or simply vanishes, and only the isotropy plays a role. When $q = 1$ the functional gives rise to the energy functional of a harmonic mapping. The relation between the new and traditional functionals will be addressed later in section 3.3.

From (1.4) the determinant of G is $g = \det(G) = \lambda_1 \lambda_2$. Let

$$(3.1) \quad \Lambda = \sqrt{\lambda_1 \lambda_2},$$

$$(3.2) \quad \mu_1(r) = \frac{\lambda_1}{\Lambda^{1/q}}, \quad \mu_2(r) = \frac{\lambda_2}{\Lambda^{1/q}}.$$

Using the symmetry assumption, we can rewrite (1.2) as

$$I_{new}[R] = \gamma \int_0^1 \left[\frac{1}{\mu_1} \left(\frac{dR}{dr} \right)^2 + \frac{1}{\mu_2} \left(\frac{R}{r} \right)^2 \right]^q r dr + (1 - 2\gamma) 2^q \int_0^1 \left[\frac{RR'}{r\sqrt{g}} \right]^q r \sqrt{g} dr.$$

Its Euler-Lagrange equation is given by

$$(3.3) \quad -\frac{\gamma}{\beta^{q-1}} \frac{d}{dr} \left(\frac{r\beta^{q-1}R'}{\mu_1} \right) + \frac{\gamma R}{r\mu_2} - \frac{(1 - 2\gamma)2^{q-1}(q-1)R}{\beta^{q-1}} \left(\frac{RR'}{r\sqrt{g}} \right)^{q-2} \frac{d}{dr} \left(\frac{RR'}{r\sqrt{g}} \right) = 0,$$

where

$$\beta = \frac{1}{\mu_1} \left(\frac{dR}{dr} \right)^2 + \frac{1}{\mu_2} \left(\frac{R}{r} \right)^2.$$

The highly nonlinear form of the new functional does not lend itself to a straightforward analytical treatment of its basic properties. Nonetheless, we devote the rest of this section to the study of several special cases of (3.3) subject to the boundary conditions (2.5). These cases are important because they help to better understand the functional and link it to the traditional one.

3.1. The exact equidistribution case ($\gamma = 0$). We first consider the case $\gamma = 0$ which corresponds to exact equidistribution. Assuming that $R(r) > 0$ for $r \in (0, 1)$, (3.3) implies

$$(3.4) \quad \frac{1}{\sqrt{g}} \frac{R}{r} \frac{dR}{dr} = \alpha,$$

where α is a constant. From (1.5), this is equivalent to

$$\frac{1}{J\sqrt{g}} = \alpha,$$

which is a multidimensional generalization of the well-known equidistribution principle in one dimension. This equation guarantees that J , the Jacobian of the coordinate transformation, does not change sign in the domain.

3.2. The pure isotropy case ($\gamma = 1/2$). For $\gamma = 1/2$ the mesh equation (3.3) reduces to

$$\frac{d}{dr} \left[\frac{\beta^{q-1} r R'}{\mu_1} \right] = \frac{\beta^{q-1} R}{r \mu_2}.$$

As in section 2.1, it is easy to show that $R(r) \geq 0$ and $R'(r) \geq 0$. Thus, for this case the mesh is also guaranteed not to cross.

In Figure 1 we depict $R'(r)$ for the traditional functional and the new functional with $\gamma = 1/2$ and several values of q . As can be seen, the mesh transformation for the new functional with different values of q is quite similar to the traditional functional. This is not surprising since for $\gamma = 1/2$ the new functional shifts all the weight towards isotropy and thus resembles the traditional functional.

3.3. The case $q = 1$. When $q = 1$, the second integral in (1.2) becomes constant. From (3.1) the mesh equation (3.3) reduces to

$$(3.5) \quad -\frac{d}{dr} \left(\frac{\Lambda r}{\lambda_1} \frac{dR}{dr} \right) + \frac{\Lambda R}{r \lambda_2} = 0.$$

Once again it is easy to prove that mesh crossing will not occur. Note that the mesh equation (3.5) is independent of the parameter γ and very similar to (2.4) for the traditional functional. In fact, for the harmonic mapping case where $\Lambda = 1$, the mesh equations (3.5) and (2.4) are identical.

For the Winslow monitor function case ($\Lambda = \lambda_1 = \lambda_2$) the mesh equation is

$$(3.6) \quad \frac{d}{dr} \left(r \frac{dR}{dr} \right) = \frac{R}{r}.$$

The solution of (3.6) compatible with the boundary conditions is $R(r) = r$. Therefore, the case $q = 1$ of the new functional method gives a trivial coordinate transformation $R = r$ and does not allow for any control of the mesh concentration when a Winslow-type monitor function is used.

Finally, for the arclength monitor function ($\lambda_2 = 1$) the mesh equation is

$$-\frac{d}{dr} \left(\frac{r}{\sqrt{\lambda_1}} \frac{dR}{dr} \right) + \frac{R}{r\sqrt{\lambda_1}} = 0.$$

This mesh equation is equivalent to that for the traditional functional (2.4) using a Winslow-type monitor function with $\sqrt{\lambda_1}$ instead of λ_1 .

In summary, except for the Winslow case, for $q = 1$ the new functional corresponds to the traditional functional with a suitable choice of the monitor function.

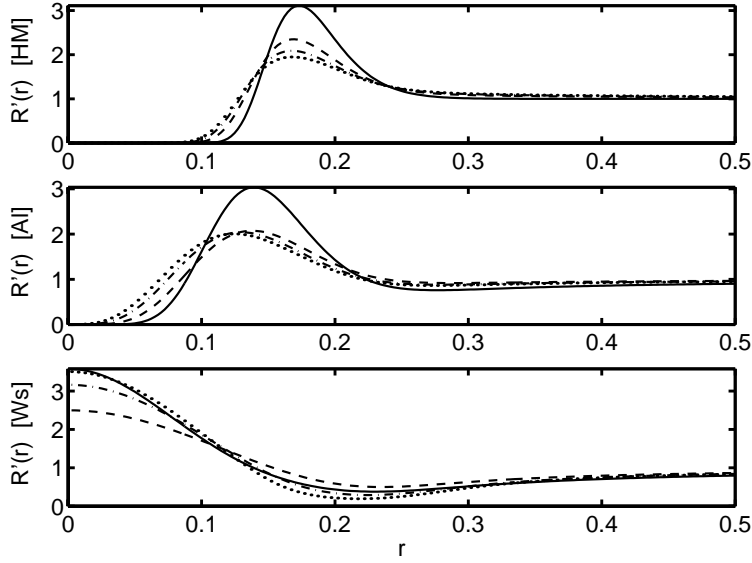


FIG. 1. Comparison of $R'(r)$ for the traditional functional (solid line) and the new functional with $\gamma = 1/2$ ($q = 2$: dashed, $q = 3$: dotted-dashed, $q = 4$: dotted). The plots correspond to the three popular choices of monitor function (harmonic mapping, arclength, and Winslow) with $\lambda_1(r) = 1 + \exp(-r^2/a)/a$ ($a = 0.01$).

4. Control of mesh density via λ_1 and λ_2 .

4.1. The traditional functional. The Euler–Lagrange equation (2.4) for the traditional functional relates the coordinate transformation to the monitor function for a given choice of λ_1 and λ_2 . The purpose of this section is to use this to show that precise control of the mesh density $D(r)$ cannot be achieved from the choice of λ_1 and λ_2 . In fact, we prove that the maximum for the mesh concentration does not occur at the maximum of λ_1 , resulting in misplacement of mesh concentration.

Let us then take (2.4) and solve for the mesh density $D(r)$ in (1.6). Motivated by the transformation (2.6) leading to the exact solution of (2.4) for the harmonic mapping monitor function ($\lambda_2 = 1/\lambda_1$), we consider the change of dependent variable

$$(4.1) \quad R(r) = e^{s(r)} \quad \text{with} \quad s(r) = \int_1^r \frac{\lambda_1(x)v(x)}{x} dx$$

for a to-be-determined and bounded function v . Substituting this into (2.4) yields the ODE for v

$$(4.2) \quad \frac{dv}{dr} = \frac{\lambda_1}{r} \left(\frac{1}{\Lambda^2} - v^2 \right).$$

It satisfies

$$(4.3) \quad v(0) = \frac{1}{\Lambda(0)},$$

since any other initial value (at $r = 0$) produces an unbounded solution v . The choice (4.3) is compatible with the special case of the harmonic mapping where $v(r) = 1$.

LEMMA 4.1. $v(r) > 0$ for all $r \in [0, 1]$.

Proof. This is an immediate result of the initial condition $v(0) = 1/\Lambda(0) > 0$ and the fact that $v' > 0$ on the line $v = 0$. □

The overall behavior of v is determined by the nullcline

$$(4.4) \quad v_{\text{null}}(r) = \frac{1}{\Lambda(r)}.$$

LEMMA 4.2. $v_{\min} \leq v(r) \leq v_{\max}$ for all $r \in [0, 1]$, where $v_{\min} = \min_r\{1/\Lambda(r)\}$ and $v_{\max} = \max_r\{1/\Lambda(r)\}$. Thus, the solution $v(r)$ is bounded by the minimum and maximum of the nullcline.

Proof. Note that $v' > 0$ below the nullcline and $v' < 0$ above it. Since $v_{\min} \leq v_{\text{null}}(r)$, we have $v' \geq 0$. This and $v(0) = 1/\Lambda(0) \geq v_{\min}$ imply that $v(r) \geq v_{\min}$. Similarly, we have $v(r) \leq v_{\max}$. □

Define r_λ as the point where λ_1 attains its maximum, i.e.,

$$\lambda_1(r_\lambda) = \max_{r \in [0,1]} \lambda_1(r).$$

We have the following lemma.

LEMMA 4.3. Let r_λ be a strict maximum point of λ_1 (so $\lambda_1''(r_\lambda) < 0$), and let $\lambda_2 = c\lambda_1^p$ for some power $p > -1$ and some constant $c > 0$. Then, $v(r_\lambda) > \frac{1}{\Lambda(r_\lambda)}$.

Proof. For this particular choice of λ_2 , we have

$$\Lambda'(r_\lambda) = 0, \quad \Lambda''(r_\lambda) \neq 0, \quad v_{\min} = \frac{1}{\Lambda(r_\lambda)}.$$

We prove the lemma by contradiction. From Lemma 4.2, we can assume only $v(r_\lambda) = 1/\Lambda(r_\lambda)$. By differentiating (4.2) twice and using the fact that $\lambda_1'(r_\lambda) = 0$, we get

$$\begin{aligned} v'(r_\lambda) &= v''(r_\lambda) = 0, \\ v'''(r_\lambda) &= -\frac{2\lambda_1(r_\lambda)\Lambda''(r_\lambda)}{r_\lambda\Lambda(r_\lambda)^3} \neq 0. \end{aligned}$$

This implies that

$$\begin{aligned} v(r) &= v(r_\lambda) + \frac{(r - r_\lambda)^3}{6}v'''(r_\lambda) + O((r - r_\lambda)^4) \\ &= v_{\min} + \frac{(r - r_\lambda)^3}{6}v'''(r_\lambda) + O((r - r_\lambda)^4). \end{aligned}$$

Hence, $v(r) < v_{\min}$ at some points in the neighborhood of r_λ , which contradicts Lemma 4.2. □

Figure 2 shows a typical vector field for v .

To study the mesh density, note that in terms of s ,

$$D(r) = \frac{R}{r} \frac{dR}{dr} = \frac{e^s}{r} s' e^s = \frac{s' e^{2s}}{r},$$

and its rate of change

$$(4.5) \quad \begin{aligned} \frac{dD}{dr} &= \frac{d}{dr} \left(\frac{s' e^{2s}}{r} \right) \\ &= \frac{e^{2s}}{r} \left(s'' + 2s'^2 - \frac{s'}{r} \right) \\ &= \frac{e^{2s}}{r^2} \left(\lambda_1' v + \lambda_1 v' - 2\frac{\lambda_1 v}{r} + 2\frac{\lambda_1^2 v^2}{r} \right). \end{aligned}$$

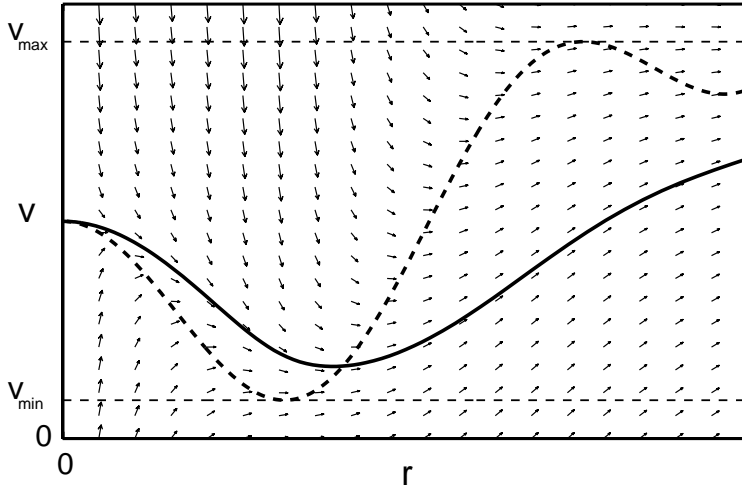


FIG. 2. Typical vector field for (4.2). The total variation $[v_{\min}, v_{\max}]$ of the nullcline (4.4) (dashed line) bounds the behavior of the solution with $v(0) = 1/\Lambda(0)$ (solid line).

Using (4.2) one obtains

$$(4.6) \quad \frac{dD}{dr} = \frac{e^{2s}}{r^2} \left\{ \lambda_1' v + \frac{\lambda_1^2}{r} \left[\left(v - \frac{1}{\lambda_1} \right)^2 + \left(\frac{1}{\Lambda^2} - \frac{1}{\lambda_1^2} \right) \right] \right\}.$$

Equation (4.6) determines where the mesh density reaches an extremum in terms of λ_1 and λ_2 . In general, it is desired that the mesh has a higher concentration of points at the maximum location of λ_1 so that the mesh concentration can be controlled by choosing λ_1 . We first consider mesh concentration at the origin $r = 0$.

THEOREM 4.1. (i) *If $\lambda_1(0) - \lambda_2(0) \neq 0$, then $D'(0)$ has the same sign as $\lambda_1(0) - \lambda_2(0)$ whether λ_1 has a maximum at $r = 0$ or not. Specifically, if $\lambda_1(0) > \lambda_2(0)$, then $D'(0) > 0$ (i.e., the mesh at the origin is coarser than in the surrounding area), and if $\lambda_1(0) < \lambda_2(0)$, then $D'(0) < 0$ (i.e., the mesh at the origin is denser than in the surrounding area).*

(ii) *Let $\lambda_2(r) = \lambda_1(r)$. If $\lambda_1'(0) \neq 0$, then $D'(0)\lambda_1'(0) > 0$. If $\lambda_1'(0) = 0$ but $\lambda_1''(0) \neq 0$, then $D'(0)\lambda_1''(0) > 0$.*

Proof. Let $y(r) = \lambda_1(r)v(r)$. Note that $y(0) = \lambda_1(0)/\Lambda(0) = \sqrt{\lambda_1(0)/\lambda_2(0)}$. Equation (4.5) can be rewritten as

$$\frac{dD}{dr} = \frac{e^{2s}}{r^2} \left(y' - \frac{2y}{r} + \frac{2y^2}{r} \right).$$

Expanding the bracketed terms on the right-hand side about $r = 0$, we get

$$(4.7) \quad \begin{aligned} \frac{dD}{dr} &= \frac{e^{2s}}{r^2} \left\{ \frac{2}{r} y(0) (y(0) - 1) + y'(0) (4y(0) - 1) + O(r) \right\} \\ &= \frac{e^{2s}}{r^2} \left\{ \frac{2}{r} \sqrt{\frac{\lambda_1(0)}{\lambda_2(0)}} \left(\sqrt{\frac{\lambda_1(0)}{\lambda_2(0)}} - 1 \right) + y'(0) \left(4\sqrt{\frac{\lambda_1(0)}{\lambda_2(0)}} - 1 \right) + O(r) \right\}. \end{aligned}$$

Thus, if $\lambda_1(0) \neq \lambda_2(0)$, the first term in the bracket dominates. In this case, $D'(r)$ has the same sign as $\lambda_1(0) - \lambda_2(0)$. The result in (i) follows.

We now prove part (ii) using (4.6). This can also be done through (4.5), but higher order terms must be used. Using the assumption $\lambda_1(r) = \lambda_2(r)$ and expanding the bracketed terms of (4.6) about $r = 0$, we get

$$\frac{dD}{dr} = \frac{e^{2s}}{r^2} \{v(0)\lambda_1'(0) + r[\lambda_1(0)v'(0) + \lambda_1'(0)(1 + v'(0)) + \lambda_1''(0)v(0)] + O(r^2)\}.$$

The results in (ii) follow since $\lambda_1'(0) = 0$ implies $v'(0) = 0$. \square

We now consider the case where mesh concentration away from the origin is desired, i.e., when $r_\lambda > 0$. Let

$$r_D : \quad D(r_D) = \max_{r \in [0,1]} D(r).$$

The following theorem shows the relative positioning of r_D with respect to r_λ .

THEOREM 4.2. *Let $r_\lambda > 0$.*

(i) *If $\lambda_1(r_\lambda) > \lambda_2(r_\lambda)$, then $D'(r_\lambda) > 0$ and thus $r_D > r_\lambda$.*

(ii) *Further, if we assume that $\lambda_2(r) = \lambda_1(r)$ (Winslow's method) and r_λ is a strict maximum point of λ_1 (i.e., $\lambda_1''(r_\lambda) < 0$), then $D'(r_\lambda) > 0$ or again $r_D > r_\lambda$.*

Proof. (i) The result is an immediate consequence of (4.6) and the assumptions.

(ii) When $\lambda_2(r) = \lambda_1(r)$, we have $\Lambda(r) = \lambda_1(r)$. Lemma 4.3, the fact that $\lambda_1(r_\lambda) = 0$, and (4.6) imply that $D'(r_\lambda) > 0$. \square

We note that a result can be obtained for the general choice of λ_2 satisfying $\lambda_2(r) = \lambda_1(r)$ only at $r = r_\lambda$. Moreover, numerical experiments (see below) show that the mismatch between r_D and r_λ for the Winslow monitor function is relatively small.

The situation with $\lambda_1(r_\lambda) < \lambda_2(r_\lambda)$ is much more complex. Note that the last term in (4.6) is now negative. In order to determine the relative positions of r_D and r_λ it is necessary to compare all the terms on the right-hand side of (4.6). It is possible for r_D and r_λ to coincide. However, numerical results (see section 4.1.4) also show that for $\lambda_2 = \lambda_1^p$ with $p > 1$, r_D can be located on either side of r_λ .

It is emphasized that part (i) of both Theorems 4.1 and 4.2 requires no explicit relationship between λ_1 and λ_2 , although we typically apply them to the monitor functions defined in (2.2).

4.1.1. The harmonic mapping case ($p = -1$). In this case, $\lambda_2 = 1/\lambda_1$. Assuming that $\lambda_1(r_\lambda) > 1$, we have $\lambda_1(r_\lambda) > \lambda_2(r_\lambda)$. Theorem 4.2 implies that $r_D > r_\lambda$, or the location of maximum mesh density is to the right of the maximum for λ_1 .

When a (local) higher mesh concentration at the origin is desired, Theorem 4.1 implies that if (a) $\lambda_1(0) > 1$, the mesh at the origin is coarser than in the surrounding area, whether λ_1 has a maximum at $r = 0$ or not. This effect is clearly depicted in Figure 3 (left column, second plot) where $r_D > r_\lambda = 0$ implies a failure to concentrate the points at the origin. If instead (b) $0 < \lambda_1(0) \leq 1$, then $\lambda_1(0) \leq \lambda_2(0)$ and the mesh will be denser in the center than in the surrounding area.

We now consider conditions under which $r_\lambda > 0$ and r_D coincide. There is a tight restriction on the choice of λ_1 since $D' = 0$ must hold where $\lambda_1' = 0$. Notice that we have $\Lambda = 1$ for the current case. Equation (4.6) implies that this can be achieved if and only if $\lambda_1(r_\lambda) = 1$. However, this cannot hold in general unless the high mesh concentration is desired only at the global maximum point and $\lambda_1(r_\lambda) = 1$ can be achieved by rescaling.

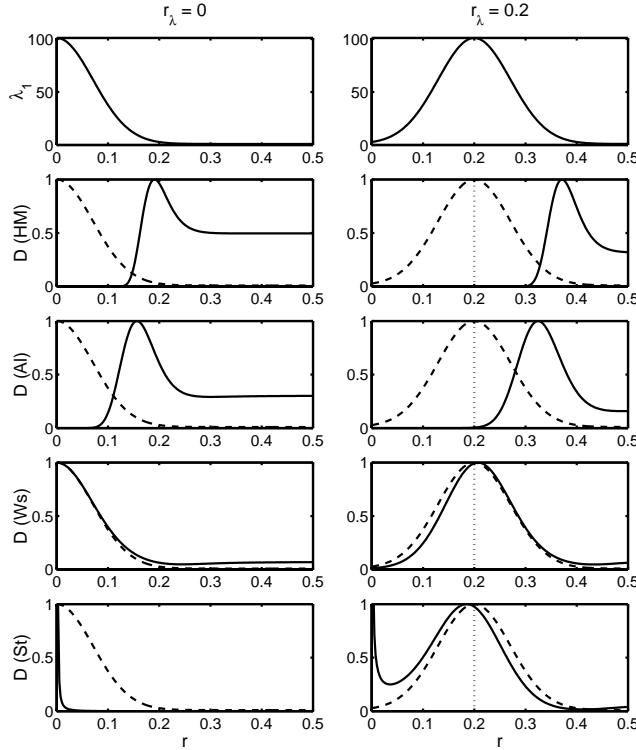


FIG. 3. Normalized mesh densities obtained with the traditional functional for different monitor functions defined in (2.2) and with $\lambda_1(r) = 1 + \exp(-(r - r_\lambda)^2/a)/a$ ($a = 0.01$) that has its maximum located at $r_\lambda = 0$ (left column) and $r_\lambda = 0.2$ (right column). The top plot depicts $\lambda_1(r)$. For guidance, we plot, along with the normalized densities (solid lines), the normalized curve for $\lambda_1(r)$ (dashed lines).

From the above analysis we see that if $\lambda_1(r_\lambda) > 1$, r_D will be located to the right of r_λ . This failure to place the higher concentration of points in the desired area is depicted in Figure 3 (right column, second plot).

4.1.2. The arclength case ($p = 0$). For the arclength case $\lambda_2(r) = 1$, a similar analysis as the one for the harmonic mapping case can be carried out. We assume $\lambda_1(r_\lambda) > 1$ since this is the one commonly used in the literature.

If $r_\lambda > 0$, Theorem 4.2 and $\lambda_1(r_\lambda) > 1 = \lambda_2$ imply that the maximum of the mesh density occurs at a location to the right of that of the maximum of λ_1 . This mismatch is illustrated in Figure 3 (right column, third plot).

The argument for $r_\lambda = 0$ is similar, and there is again a mismatch (to the right) between the locations of the maxima of the mesh density and λ_1 (see Figure 3, left column, third plot).

4.1.3. The Winslow case ($p = 1$). If a high mesh concentration is desired at a strict maximum point $r_\lambda > 0$ of λ_1 , Theorem 4.2 implies that r_D will be located to the right of r_λ . Nevertheless, as Figure 3 (right column, fourth plot) shows, the mismatch between the maxima for D and λ_1 can be very small (compared with the other cases).

On the other hand, Theorem 4.1 implies that the mesh has higher concentration

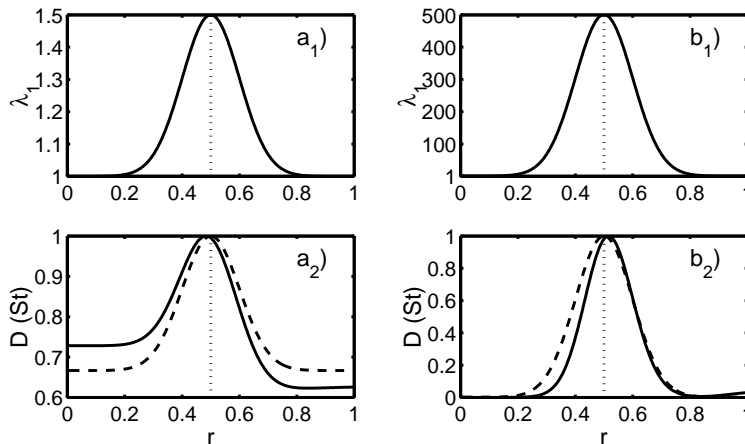


FIG. 4. Normalized mesh densities obtained with the traditional functional for the strong concentration case ($p = 2$) with $\lambda_1(r) = 1 + A \exp(-(r - r_\lambda)^2/a)/a$ ($a = 0.02$, $r_\lambda = 0.5$) and (a) $A = 0.01$ and (b) $A = 10$. The top plots show $\lambda_1(r)$. For guidance, in a_2 and b_2 we plot the normalized curve for $\lambda_1(r)$ (dashed lines) along with the normalized densities (solid lines).

at $r = 0$ if either $\lambda_1'(0) < 0$ or $r = 0$ is a local maximum point of λ_1 . Figure 3 (left column, fourth plot) shows good agreement between the shape of λ_1 and the mesh density.

4.1.4. The strong concentration case ($p = 2$). Consider first the case where a higher mesh concentration at the origin is desired. Theorem 4.1 implies that the maximum for the mesh density is located at the origin if $\lambda_1(0) > 1$ (see the last plot in Figure 3, left column). However, the rate of change of the density may be a very large negative value—proportional to $\lim_{r \rightarrow 0} e^{2s}/r^3$. This effect is observed in Figure 3 (last plot, left column) where the mesh density is very steep at the origin, giving an overconcentration of points at $r = 0$. Incidentally, our use of the term “strong concentration” for the $p = 2$ case reflects this behavior.

For $r_\lambda > 0$, the current situation is more complex than the previous cases and Theorem 4.2 does not apply if $\lambda_1(r_\lambda) > 1$. Figure 4 shows that r_D can be located to either side of r_λ . Since in this case we have $\lambda_1(0) < \lambda_2(0)$, Theorem 4.1 implies that the mesh concentration has a maximum at the origin. Thus, it is possible for the mesh concentration to have two (or more) maxima, one near the desired location r_λ and a spurious (and steep) maximum at $r = 0$ (see the last plot in Figure 3, right column).

4.2. The new functional. The Euler–Lagrange equation (3.3) corresponding to the new functional is too complex to carry out an analysis similar to the one for the traditional functional, and we instead perform a numerical study of the relation between the monitor function (λ_1 and λ_2) and the mesh density $D(r)$. In particular, we show that by appropriate control of the weighting γ between isotropy and equidistribution it is possible to reduce the mismatch between the location of the maximum for the monitor function and that of the maximum for $D(r)$. As for the traditional functional, we concentrate our attention on monitor functions of the type (2.1) and use the same notation as in (2.2) to designate the most popular choices of p . Note that for the harmonic mapping monitor function $g = 1$, and equidistribution reads as $J = \text{constant}$, giving no mesh control in the new functional. As a result, it is expected

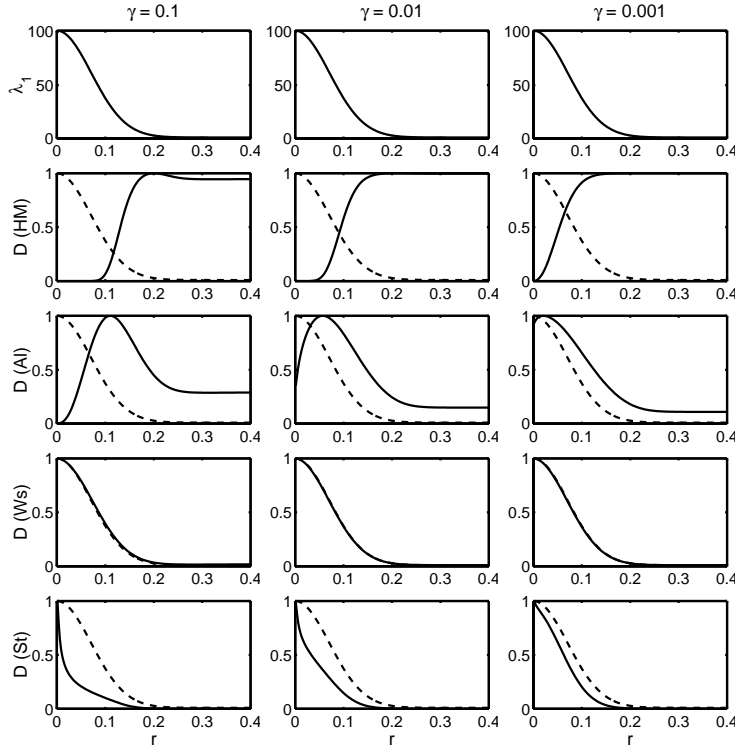


FIG. 5. Normalized mesh densities (solid lines) obtained with the new functional for a monitor function (dashed lines) such that $\lambda_1(r) = 1 + \exp(-(r - r_\lambda)^2/a)/a$ ($a = 0.01$, $r_\lambda = 0$) for different choices of λ_2 and γ ($q = 2$).

that the new functional combined with the harmonic mapping monitor function gives no better results than those with the traditional functional, even for a small value of γ .

4.2.1. Concentration at $r = 0$. For $r_\lambda = 0$, Figure 5 shows the monitor function and the mesh density for the various choices of monitor function (2.2) and weighting between isotropy and equidistribution. For large γ (close to $1/2$), the new functional tends to emphasize isotropy, giving similar results to those for the traditional functional. For $\gamma = 0.1$ (first column in Figure 5), the harmonic mapping and the arclength monitor functions tend to misplace the position of the maximum for the density as before. For the Winslow and strong concentration cases, $D(r)$ achieves its maximum at $r = 0$.

Decreasing γ puts more weight on equidistribution, allowing for a better distribution of the mesh density. In fact, by decreasing γ (second and third columns in Figure 5) the maximum for the mesh density is pulled towards the correct position $r = 0$. As pointed out above, the harmonic mapping case fails to have its maximum at $r = 0$ even for very small γ . For the other cases ($p \geq 0$), as γ tends to zero, not only the mesh density has its maximum placed correctly, but its shape tends to mimic the shape of λ_1 . This suggests that for small γ it is possible to control the position of the maximum mesh concentration as well as the shape of the mesh density from the choice of monitor function. Interestingly, the Winslow case provides the best control

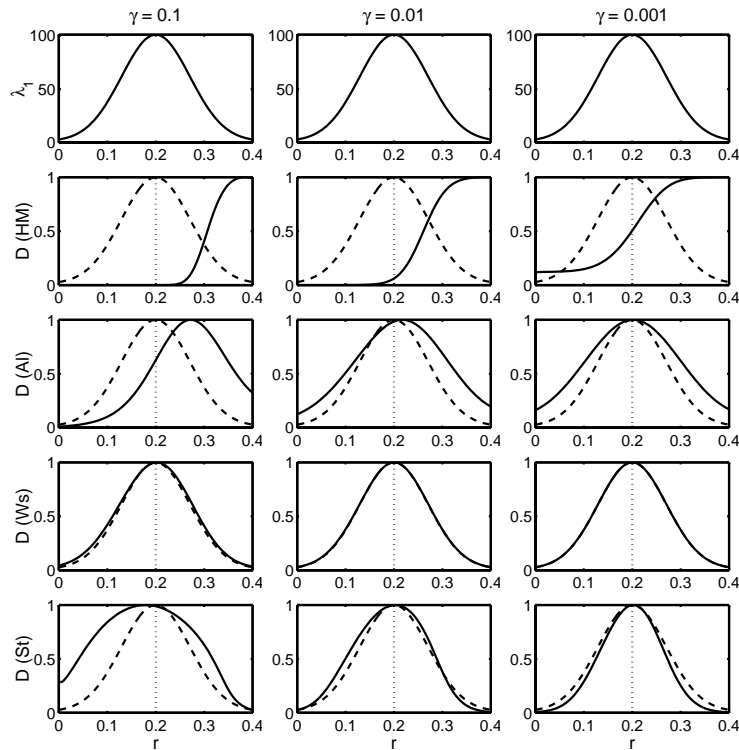


FIG. 6. Normalized mesh densities (solid lines) obtained with the new functional for a monitor function (dashed lines) such that $\lambda_1(r) = 1 + \exp(-(r-r_\lambda)^2/a)/a$ ($a = 0.001$, $r_\lambda = 0.2$) for different choices of λ_2 and γ ($q = 2$).

on the mesh density, and for small γ ($\gamma < 0.01$) $D(r)$ is almost indistinguishable from $\lambda_1(r)$.

4.2.2. Concentration at $r > 0$. For $r_\lambda > 0$ we obtain similar results to those for the traditional functional when using a large value of γ (see left column in Figure 6). In particular, the position of the mesh density maximum does not coincide with r_λ except in the Winslow case. As we decrease γ , the new functional weights more towards equidistribution, and the location of the maximum for $D(r)$ tends to approach r_λ , again reinforcing the observation that for small γ and $p \geq 0$ it is possible to have a good control on the mesh density (maximum and shape) from the monitor function.

5. Numerical results. In this section we present some numerical results obtained with the functionals (1.1) and (1.2). For simplicity, square physical and computational domains and structured meshes are used in the computation. As a consequence, axially symmetric meshes are not generated. Nevertheless, the numerical results are sufficient to support the analysis of the previous sections and highlight the level of control of mesh concentration through the monitor functions.

The (two-dimensional) Euler–Lagrange equations for functionals (1.1) and (1.2) are discretized with central finite differences and solved using the moving mesh PDE approach [5, 7]. With this approach, a derivative $(\partial \mathbf{x})/(\partial t)$ (where $\mathbf{x} = (x, y)^T$) with respect to pseudotime t is added to the Euler–Lagrange equation, and the resulting

parabolic system is integrated using a modified backward Euler scheme with which the coefficients of terms $(\partial \mathbf{x})/(\partial \xi^i)$ and $(\partial^2 \mathbf{x})/(\partial \xi^i \partial \xi^j)$ are calculated at the previous time level. The linear algebraic system is solved using a preconditioned conjugate gradient method. The converged mesh is obtained when the root-mean-square norm of the residual is less than 10^{-4} . All computations start with a uniform mesh of size 41×41 and use a uniform boundary correspondence between Ω and Ω_c . We use $q = 2$ in all cases and, following the common practice, choose λ_1 to be greater than 1.

Example 5.1. The first example is to generate adaptive meshes for the monitor function (1.4) with

$$(5.1) \quad \lambda_1 = 1 + \frac{1}{a} e^{-(r-0.2)^2/a},$$

where $r = \sqrt{x^2 + y^2}$ and $a = 0.01$. In the (x, y) coordinate system, G has the form

$$(5.2) \quad G = \frac{\lambda_1}{x^2 + y^2} \begin{pmatrix} x^2 & xy \\ xy & y^2 \end{pmatrix} + \frac{\lambda_2}{x^2 + y^2} \begin{pmatrix} y^2 & -xy \\ -xy & x^2 \end{pmatrix}.$$

The goal is to generate meshes with higher point concentration around the circle $x^2 + y^2 = 0.2^2$.

The meshes obtained are shown in Figures 7 and 8. The first row corresponds to the traditional functional, while the second, third, and fourth rows are for the new functional with $\gamma = 0.5, 0.1$ and 0.01 , respectively. Each column is associated with a given monitor function.

The left column of Figure 7 shows that the mesh concentration is badly misplaced for both the traditional and new functionals using the harmonic mapping monitor function ($p = -1$). In this case the traditional functional gives exactly the harmonic mapping method used by Dvinsky [4]. Note that the new functional does not work well, as expected, since $g = 1$ and $J = \text{constant}$, giving no control of mesh concentration.

For the arclength monitor function ($p = 0$, the right column of Figure 7), the traditional functional still produces the mismatched concentration. However, since $g = \lambda$ and the equidistribution becomes $J\sqrt{\lambda} = \text{constant}$, the new functional bears the feature of equidistribution and leads to the correct concentration when a small value of γ is used.

Interestingly, with the Winslow-type monitor function, both the traditional and new functionals generate correct mesh concentration—see the left column of Figure 8. For the case of strong concentration with $p = 2$ (see the right column of Figure 8), the new functional produces the correct results, whereas the traditional one seems to overconcentrate mesh points inside the circle $x^2 + y^2 = 0.2^2$, although there is also concentration around the circle.

From these two figures one can also see that the new functional with $\gamma = 0.5$ leads to results similar to but slightly less adaptive than those obtained with the traditional functional.

Example 5.2. The second example is to generate adaptive meshes for the monitor function (1.4) with

$$(5.3) \quad \lambda_1 = 1 + \frac{1}{a} e^{-r^2/a}, \quad a = 0.01.$$

The goal is now to generate adaptive meshes with higher point concentration at the origin.

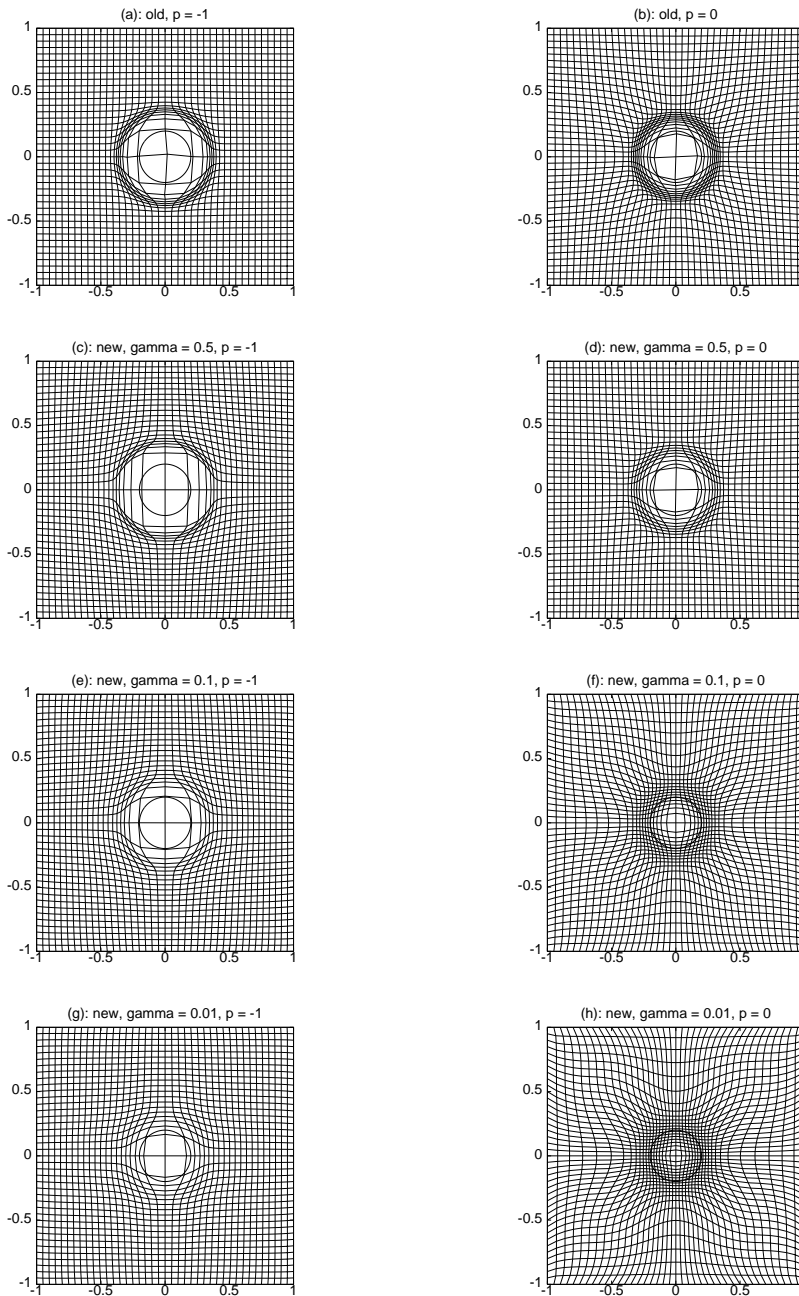


FIG. 7. Adaptive meshes are obtained for Example 5.1 with the harmonic mapping ($p = -1$) and arclength ($p = 0$) monitor functions. Desirable mesh point concentration is around the circle $x^2 + y^2 = 0.2^2$ (the bold solid circle).

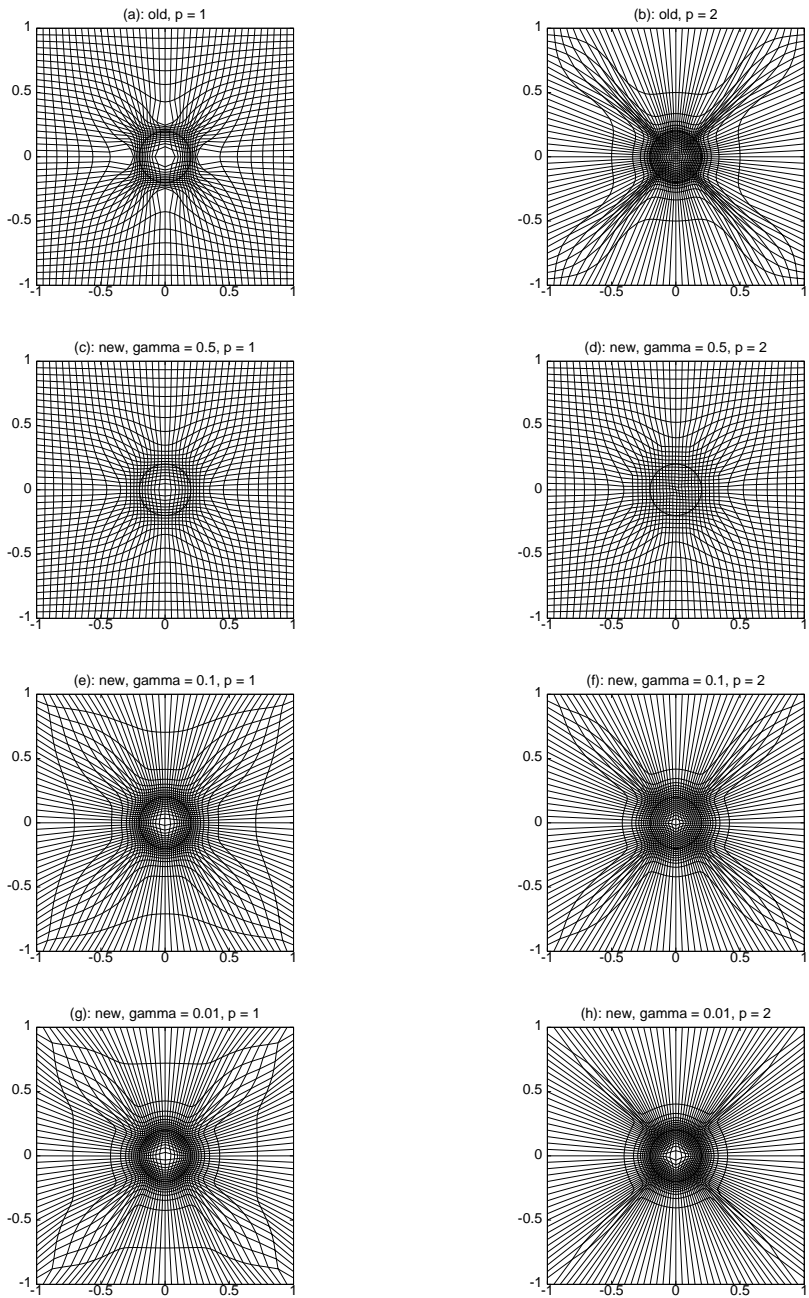


FIG. 8. Adaptive meshes are obtained for Example 5.1 with the Winslow-type ($p = 1$) and strong concentration ($p = 2$) monitor functions. Desirable mesh point concentration is around the circle $x^2 + y^2 = 0.2^2$ (the bold solid circle).

The meshes obtained are shown in Figures 9 and 10. The results confirm the observations made in Example 5.1 and the analysis given in the preceding sections. That is, the traditional functional misplaces meshes for the harmonic mapping and arc-length monitor functions and correctly places them for the Winslow-type and strong concentration monitor functions; the new functional with $\gamma = 0.5$ leads to meshes similar to but slightly less adaptive than those obtained with the traditional functional; and the new functional with a small value of γ leads to meshes with correct concentration when the arclength, Winslow-type, or strong concentration monitor function is used.

6. The traditional functional for spherically symmetric problems. A similar analysis can be carried out for the traditional functional applied to spherically symmetric problems in three dimensions. Consider

$$(6.1) \quad I_{trad}[\xi, \eta, \zeta] = \int_{\Omega} (\nabla \xi^T G^{-1} \nabla \xi + \nabla \eta^T G^{-1} \nabla \eta + \nabla \zeta^T G^{-1} \nabla \zeta) \, dx dy dz,$$

where $\Omega = \{(x, y, z) \mid x^2 + y^2 + z^2 < 1\}$. Take $\Omega_c = \{(\xi, \eta, \zeta) \mid \xi^2 + \eta^2 + \zeta^2 < 1\}$, and let the spherical coordinates for Ω and Ω_c be

$$\begin{cases} x = r \sin(\theta) \cos(\phi), \\ y = r \sin(\theta) \sin(\phi), \\ z = r \cos(\theta), \end{cases} \quad \begin{cases} \xi = R \sin(\Theta) \cos(\Phi), \\ \eta = R \sin(\Theta) \sin(\Phi), \\ \zeta = R \cos(\Theta). \end{cases}$$

Consider the case where the physical solution is spherically symmetric. Assume that the corresponding mesh adaptation is also spherically symmetric, i.e.,

$$(6.2) \quad R = R(r), \quad \Theta = \theta, \quad \Phi = \phi.$$

Then it is reasonable to use the monitor function in the form

$$(6.3) \quad G = \lambda_1(r) \mathbf{e}_r \mathbf{e}_r^T + \lambda_2(r) \mathbf{e}_\theta \mathbf{e}_\theta^T + \lambda_3(r) \mathbf{e}_\phi \mathbf{e}_\phi^T,$$

where \mathbf{e}_r , \mathbf{e}_θ , and \mathbf{e}_ϕ are the unit vectors in the radial, latitudinal, and longitudinal axes. Under the symmetry assumption, (6.1) reduces to

$$I_{trad}[R] = \int_0^1 \left[\frac{1}{\lambda_1} \left(\frac{dR}{dr} \right)^2 + \frac{2}{\lambda_{23}} \left(\frac{R}{r} \right)^2 \right] r^2 dr,$$

where λ_{23} is defined as

$$\frac{2}{\lambda_{23}} = \frac{1}{\lambda_2} + \frac{1}{\lambda_3}.$$

The corresponding boundary value problem is given by

$$(6.4) \quad \begin{aligned} -\frac{d}{dr} \left(\frac{r^2}{\lambda_1} \frac{dR}{dr} \right) + \frac{2}{\lambda_{23}} R &= 0, \\ R(0) &= 0, \quad R(1) = 1. \end{aligned}$$

The transformation (4.1) can be used for analyzing (6.4). We obtain the equation for v

$$(6.5) \quad v' = \frac{\lambda_1}{r} \left(\frac{2}{\lambda_1 \lambda_{23}} - \frac{v}{\lambda_1} - v^2 \right)$$

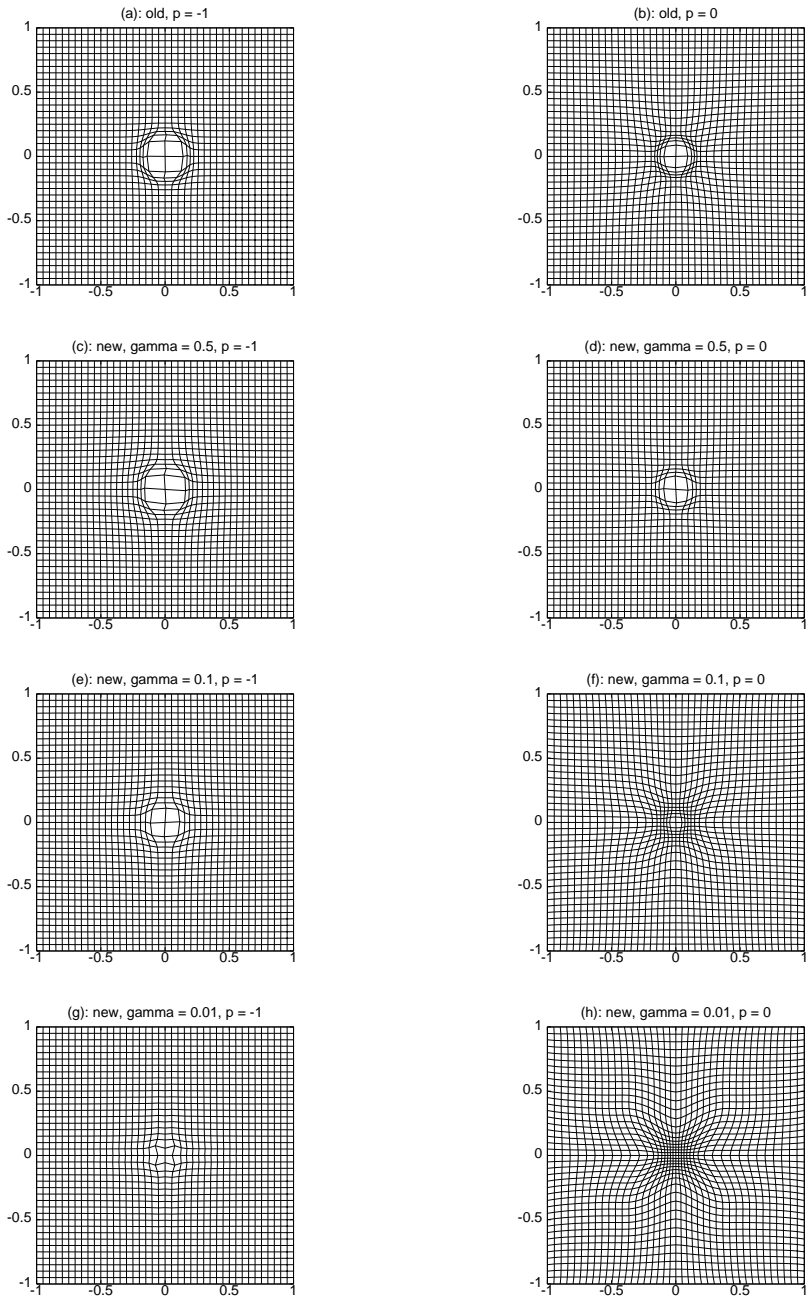


FIG. 9. Adaptive meshes are obtained for Example 5.2 with the harmonic mapping ($p = -1$) and arclength ($p = 0$) monitor functions. Desirable mesh point concentration is near the origin.

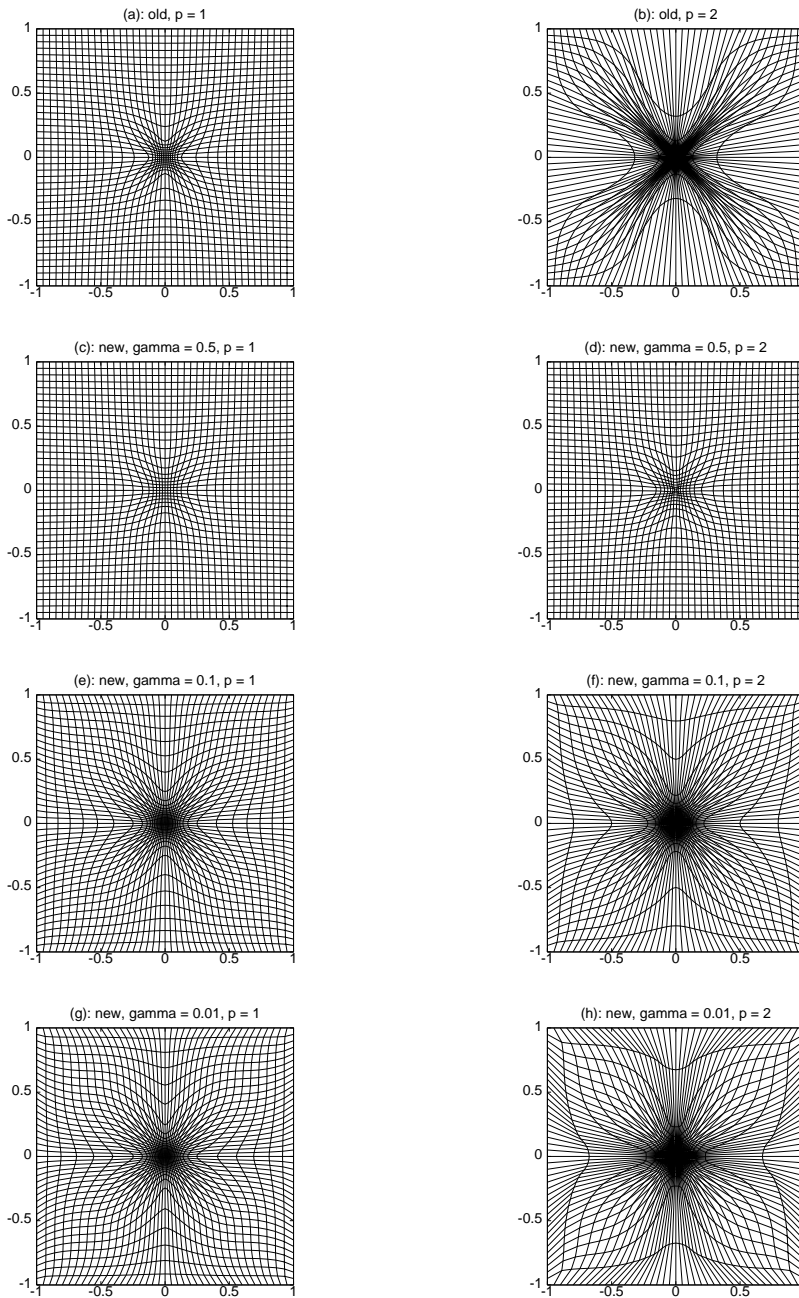


FIG. 10. Adaptive meshes are obtained for Example 5.2 with the Winslow-type ($p = 1$) and strong concentration ($p = 2$) monitor functions. Desirable mesh point concentration is near the origin.

which is subject to the initial condition

$$(6.6) \quad v(0) = \frac{1}{2} \sqrt{\frac{1}{\lambda_1(0)^2} + \frac{8}{\lambda_1(0)\lambda_{23}(0)}} - \frac{1}{2\lambda_1(0)}.$$

It is straightforward to show that the solution v of (6.5) has the properties stated in Lemmas 4.1–4.3.

In the current situation, the mesh density has the form

$$D(r) = \frac{R^2}{r^2} \frac{dR}{dr}.$$

Its rate of change reads as

$$(6.7) \quad \begin{aligned} D'(r) &= \frac{e^{3s}}{r^3} \left[(\lambda_1 v)' - \frac{3(\lambda_1 v)}{r} + \frac{3(\lambda_1 v)^2}{r} \right] \\ &= \frac{e^{3s}}{r^3} \left[\lambda_1' v + \frac{2\lambda_1^2}{r} \left(\left(v - \frac{1}{\lambda_1} \right)^2 + \left(\frac{1}{\lambda_1 \lambda_{23}} - \frac{1}{\lambda_1^2} \right) \right) \right]. \end{aligned}$$

We have the following theorems which are basically identical to Theorems 4.1 and 4.2. One may notice that in this three-dimensional case, the relation between λ_1 and λ_{23} , rather than those between λ_1 and each of λ_2 and λ_3 , plays a role in affecting the corresponding mesh adaptation.

THEOREM 6.1. (i) *If $\lambda_1(0) - \lambda_{23}(0) \neq 0$, then $D'(0)$ has the same sign as $\lambda_1(0) - \lambda_{23}(0)$, whether $r = 0$ is a maximum point of λ_1 or not.*

(ii) *Let $\lambda_{23}(r) = \lambda_1(r)$. If $\lambda_1'(0) \neq 0$, then $D'(0)\lambda_1'(0) > 0$. If $\lambda_1'(0) = 0$ but $\lambda_1''(0) \neq 0$, then $D'(0)\lambda_1''(0) > 0$.*

THEOREM 6.2. *Let $r_\lambda > 0$.*

(i) *If $\lambda_1(r_\lambda) > \lambda_2(r_\lambda)$, then $D'(r_\lambda) > 0$ and thus $r_D > r_\lambda$.*

(ii) *Further, if we assume that $\lambda_{23}(r) = \lambda_1(r)$ and r_λ is a strict maximum point of λ_1 (i.e., $\lambda_1''(r_\lambda) < 0$), then $D'(r_\lambda) > 0$ or $r_D > r_\lambda$.*

7. Conclusions and comments. The question of how variational grid generators behave when solving problems with axisymmetric solutions has been investigated. Specifically, two functionals have been analyzed in the previous sections for their abilities to precisely control the mesh concentration via monitor functions. One is the traditional functional (1.1) which includes Winslow’s method and Dvinsky’s method of harmonic mappings as special cases. The other is the new functional (1.2) proposed by Huang in [6] which explicitly includes the isotropy (or regularity) and equidistribution features. The analysis is primarily done for axisymmetrical problems in two dimensions. For axially symmetric mesh adaptation, it is reasonable to use a monitor function of the form in (1.4).

Theoretical results for the traditional functional are given in Theorems 4.1 and 4.2. Specifically, when higher mesh concentration at the origin is desired, a choice of the radial and angular components λ_1 and λ_2 of the monitor function satisfying $\lambda_1(0) < \lambda_2(0)$ will make the mesh denser at $r = 0$ than in the surrounding area whether or not λ_1 has a maximum value at $r = 0$. The purpose can also be served by choosing λ_1 to have a local maximum at $r = 0$ when a Winslow-type monitor function with $\lambda_1(r) = \lambda_2(r)$ is employed. Unfortunately, the choice $\lambda_2(r) = \lambda_1(r)^p$ with $p < 0$, which includes Dvinsky’s method of harmonic mappings and the arclength monitor function as special cases, will not satisfy the condition $\lambda_1(0) < \lambda_2(0)$ if $\lambda_1(0) > 1$ (as

commonly taken in the literature) and leads to a mesh with coarser concentration of points in the center than in the surrounding area.

On the other hand, when higher mesh concentration around a ring $r = r_\lambda > 0$ is desired, the traditional functional provides far less control by choosing λ_1 and λ_2 . Indeed, Theorem 4.2 shows that there surely is a mismatch between the position r_λ of the maximum of λ_1 and the location r_D of the maximum of the mesh density if either (a) $\lambda_1(r_\lambda) > \lambda_2(r_\lambda)$ (which is the case for the harmonic mapping or the arclength monitor function with $\lambda_1(r_\lambda) > 1$) or (b) a Winslow-type monitor function is used and r_λ is a strict maximum point of λ_1 . Moreover, a mismatch between r_D and r_λ is also possible for the case $\lambda_1(r_\lambda) < \lambda_2(r_\lambda)$. Indeed, the numerical results show that r_D can be located to either side of r_λ when $\lambda_1(r_\lambda) > 1$ and λ_2 is taken as $\lambda_2 = \lambda_1^p$ for $p > 1$. Nevertheless, the numerical results suggest that $|r_D - r_\lambda|$ is relatively small for the Winslow case $\lambda_2 = \lambda_1$. The analysis also shows that for the harmonic mapping case $\lambda_2 = 1/\lambda_1$, r_D can be made to agree with r_λ by rescaling λ_1 such that $\lambda_1(r_\lambda) = 1$. However, this can be done if the mesh concentration is needed only at the location of the (global) maximum of λ_1 .

For axially symmetric problems, the new functional leads to a nonlinear mesh equation too complex to permit an analysis like that for the traditional functional. Nevertheless, numerical results presented in sections 4 and 5 show that the new functional offers explicit control for mesh concentration by adjusting the value of γ that weights the isotropy and equidistribution. Specifically, when using a large value of γ (close to $1/2$) we obtain similar results to those for the traditional functional cases. However, as we decrease γ , the new functional weights more towards equidistribution, and both the location of the maximum and the profile of the mesh density tend to coincide with those of λ_1 for a monitor function with a nonconstant determinant. For the case of the harmonic mapping monitor function, the determinant is $g = 1$ and equidistribution becomes $J = \text{constant}$ so no control of mesh concentration is possible by choosing λ_1 . Thus, as expected, the new functional does not work in this case even when a small value of γ is used.

Analysis has also been carried out for the traditional functional applied to spherically symmetric problems in three dimensions. The results are stated in Theorems 6.1 and 6.2.

In the future we intend to investigate a number of higher-dimensional axisymmetrical problems arising in physical applications and show the practicability of the methods which have performed well here.

Acknowledgment. The authors are grateful to the referees for their valuable comments.

REFERENCES

- [1] J. U. BRACKBILL AND J. S. SALTZMAN, *Adaptive zoning for singular problems in two dimensions*, J. Comput. Phys., 46 (1982), pp. 342–368.
- [2] W. CAO, W. HUANG, AND R. D. RUSSELL, *A study of monitor functions for two-dimensional adaptive mesh generation*, SIAM J. Sci. Comput., 20 (1999), pp. 1978–1994.
- [3] C. DE BOOR, *Good approximation by splines with variable knots II*, in Proceedings of the Conference on the Numerical Solution of Differential Equations, Dundee, Scotland, 1973, Lecture Notes in Math. 363, G. A. Watson, ed., Springer-Verlag, Berlin, 1974, pp. 12–20.
- [4] A. S. DVINSKY, *Adaptive grid generation from harmonic maps on Riemannian manifolds*, J. Comput. Phys., 95 (1991), pp. 450–476.
- [5] W. HUANG, *Practical aspects of formulation and solution of moving mesh partial differential equations*, J. Comput. Phys., 171 (2001), pp. 753–775.

- [6] W. HUANG, *Variational mesh adaptation: Isotropy and equidistribution*, J. Comput. Phys., 174 (2001), pp. 903–924.
- [7] W. HUANG AND R. D. RUSSELL, *A high dimensional moving mesh strategy*, Appl. Numer. Math., 26 (1997), pp. 63–76.
- [8] W. HUANG AND W. SUN, *Variational mesh adaptation II: Error estimates and monitor functions*, J. Comput. Phys., to appear.
- [9] P. KNUPP, *Mesh generation using vector-fields*, J. Comput. Phys., 119 (1995), pp. 142–148.
- [10] P. M. KNUPP, *Jacobian-weighted elliptic grid generation*, SIAM J. Sci. Comput., 17 (1996), pp. 1475–1490.
- [11] P. M. KNUPP AND N. ROBIDOUX, *A framework for variational grid generation: Conditioning the Jacobian matrix with matrix norms*, SIAM J. Sci. Comput., 21 (2000), pp. 2029–2047.
- [12] W. REN AND X.-P. WANG, *An iterative grid redistribution method for singular problems in multiple dimensions*, J. Comput. Phys., 159 (2000), pp. 246–273.
- [13] S. STEINBERG AND P. J. ROACHE, *Variational grid generation*, Numer. Methods Partial Differential Equations, 2 (1986), pp. 71–96.
- [14] A. WINSLOW, *Numerical solution of the quasi-linear Poisson equation in a nonuniform triangle mesh*, J. Comput. Phys., 1 (1967), pp. 149–172.
- [15] A. M. WINSLOW, *Adaptive Mesh Zoning by the Equipotential Method*, Technical report UCID-19062, Lawrence Livermore Laboratory, Livermore, CA, 1981.